Supporting Information

$Au_5Ag_{12}(SR)_9(dppf)_4$ alloy nanocluster: Structural determination, optical property and photothermal effect investigation

Jiawei Wang,[a] Along Ma,[a,b] Yonggang Ren,[a] Xuekairui Shen,[a] Yifei Wang,[a] Caixia Song *[a] and Shuxin Wang *[a,b]

[a]College of Materials Science and Engineering, Qingdao University of Science and Technology, Qingdao 266042, P. R. China.

[b]Shandong Key Laboratory of Biochemical Analysis, College of Chemistry and Molecular Engineering, Qingdao University of Science and Technology, Qingdao 266042, P. R. China.

*Corresponding author, e-mail: songcaixia@qust.edu.cn (Caixia Song); shuxin_wang@qust.edu.cn (Shuxin Wang)

Table of Contents

Section 1. Supporting Figures

Au_4Ag_{13} and **Au_7Ag_8** nanoclusters.
Figure S17. Temperature-dependent PL spectra of **Au_5Ag_{12}** nanocluster from 1100 nm to 2500 nm in 2-MeTHF from 300 K to 80 K.
Figure S18. Simplified Jablonski diagram illustrating photophysical processes of **Au_5Ag_{12}** nanocluster.
Figure S19. Time dependent images of **Au_5Ag_{12}** solutions of different concentrations (0.1 mM, 0.05 mM, and 0.01 mM) upon laser irradiation, followed by a cooling period.
Figure S20. The photothermal stability of **Au_5Ag_{12}** nanoclusters at different concentrations was monitored by UV-vis spectroscopy.
Figure S21. Temperature change of blank $CHCl_3$ solvent.
Figure S22. Absorption spectra of **Au_5Ag_{12}**, **Au_5Ag_{11}**, **Au_7Ag_8** nanoclusters.
Figure S23. Fluorescence decay profile of **Au_4Ag_{13}**, **Au_7Ag_8** and **Au_5Ag_{11}** nanoclusters.
Figure S24. The time-dependent temperature of the four AuAg alloy nanoclusters solutions (0.1 mM) during laser irradiation at 808 nm with different power.
Figure S25. The time-dependent temperature of the four AuAg alloy nanoclusters solutions (0.1 mM) during laser irradiation at 1.4 W cm^{-2} with different wavelengths.
Figure S26. Photothermal cycling measurement and corresponding UV-vis spectra of **Au_5Ag_{12}** solutions (0.1 mM, 0.05 mM, 0.01 mM).
Figure S27. Photothermal cycling measurement and corresponding UV-vis spectra of **Au_5Ag_{11}**, **Au_4Ag_{13}** and **Au_7Ag_8** nanoclusters in $CHCl_3$.
Figure S28. Monitoring the stability of **Au_5Ag_{12}**, **Au_5Ag_{11}**, **Au_4Ag_{13}** and **Au_7Ag_8** nanoclusters in $CHCl_3$ within 14 days.

Section 2. Supporting Table

Table S1. The crystal structure parameters for **$Au_5Ag_{12}(SR)_9(dppf)_4$**.
Table S2. The corresponding PLQY, τ, k_R and k_{NR} of **Au_4Ag_{13}**, **Au_7Ag_8**, and **Au_5Ag_{11}** nanoclusters.

Section 1. Supporting Figures

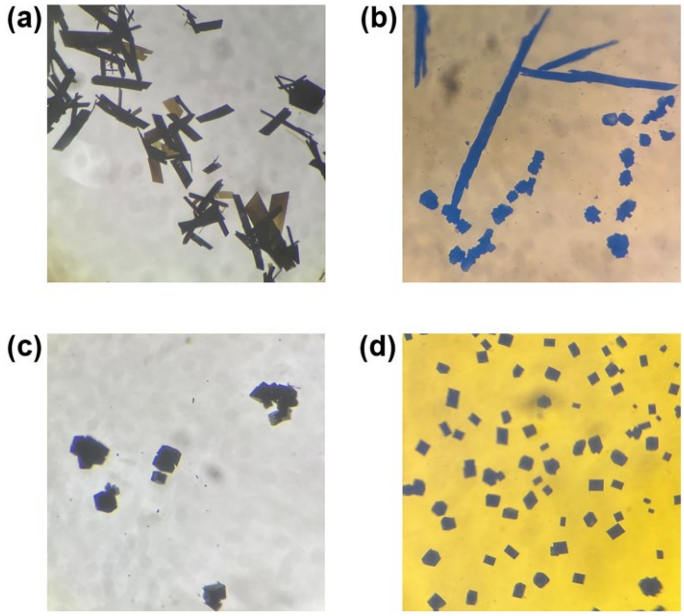

Figure S1. The optical microscopic image of the single crystals of the $\mathbf{Au_5Ag_{12}}$, $\mathbf{Au_5Ag_{11}}$, $\mathbf{Au_4Ag_{13}}$ and $\mathbf{Au_7Ag_8}$ nanoclusters. (a) $\mathbf{Au_5Ag_{12}}$; (b) $\mathbf{Au_5Ag_{11}}$; (c) $\mathbf{Au_4Ag_{13}}$; (d) $\mathbf{Au_7Ag_8}$.

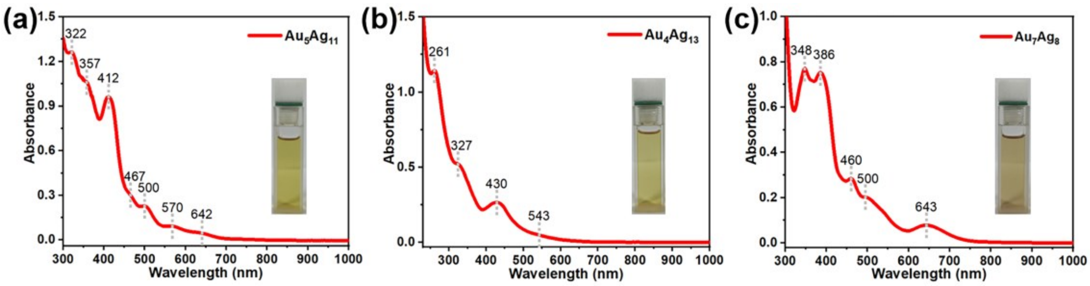

Figure S2. The UV-vis absorbance spectra of the $\mathbf{Au_5Ag_{11}}$, $\mathbf{Au_4Ag_{13}}$ and $\mathbf{Au_7Ag_8}$ nanoclusters in CH_2Cl_2 (Insets are the photos of three nanoclusters in CH_2Cl_2). (a) $\mathbf{Au_5Ag_{11}}$; (b) $\mathbf{Au_4Ag_{13}}$; (c) $\mathbf{Au_7Ag_8}$.

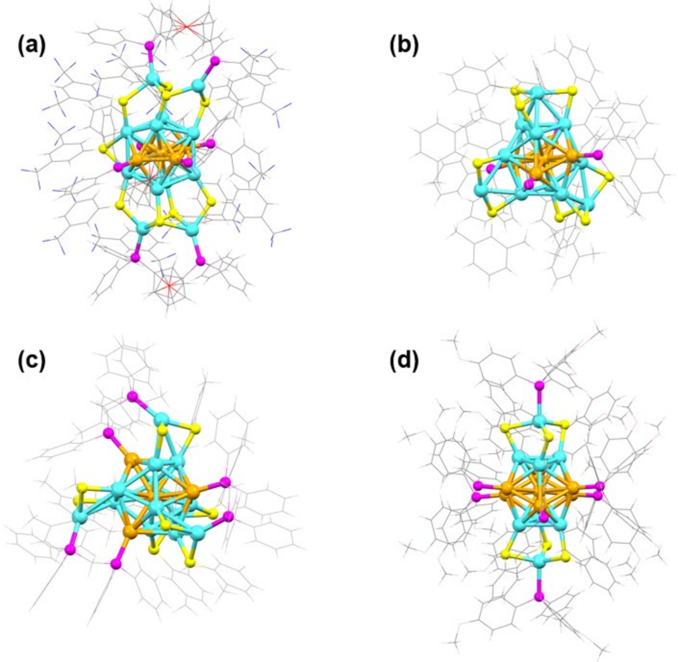

Figure S3. The overall structure of the **Au_5Ag_{12}**, **Au_5Ag_{11}**, **Au_4Ag_{13}** and **Au_7Ag_8** nanoclusters. (a) **Au_5Ag_{12}**; (b) **Au_5Ag_{11};** (b) **Au_4Ag_{13};** (d) **Au_7Ag_8**. Color labels: orange = Au; light blue = Ag; red = Fe; yellow = S; magenta = P; pink = O; grey = C; white = H.

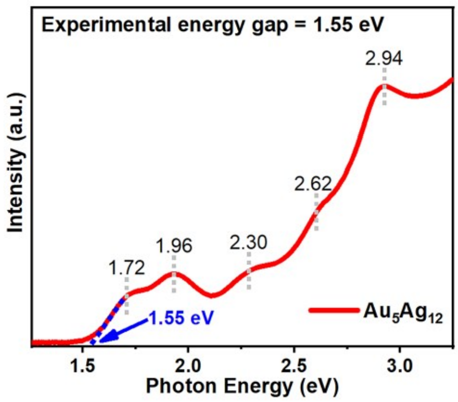

Figure S4. UV-vis absorption spectrum (photon energy scale) of the **Au_5Ag_{12}** nanocluster in CH_2Cl_2. The experimental energy gap of the **Au_5Ag_{12}** nanocluster in CH_2Cl_2 was determined as ~1.55 eV.

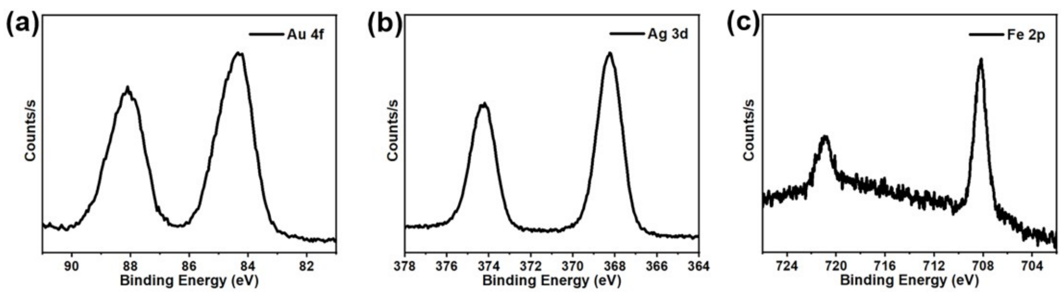

Figure S5. XPS spectra of the **Au_5Ag_{12}** nanocluster. (a)Au 4f; (b) Ag 3d; (c) Fe 2p.

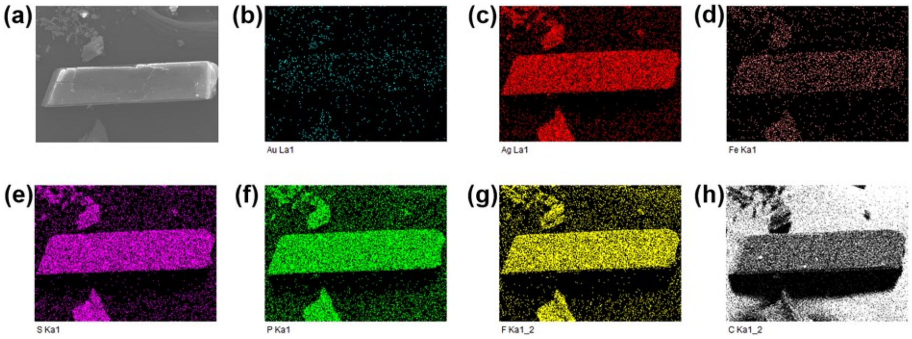

Figure S6. SEM image and corresponding elemental mapping images of **Au_5Ag_{12}** nanocluster. (a) SEM image of a small deformed single crystal; (b)-(h) Elemental mapping images of Au, Ag, Fe, S, P, F, and C, respectively.

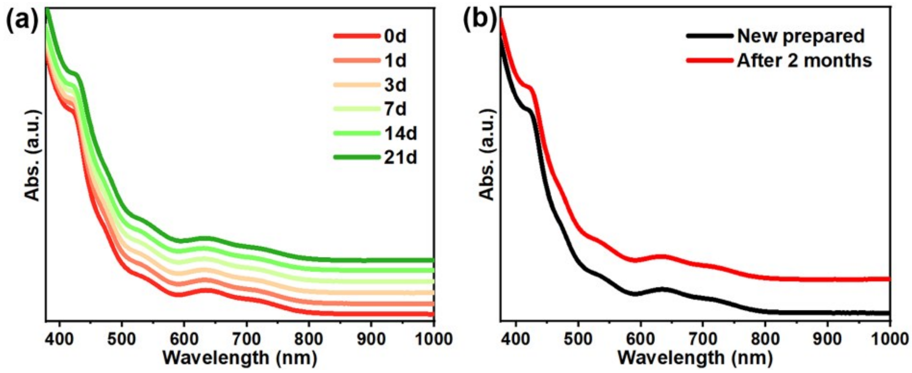

Figure S7. Monitoring the stability of **Au_5Ag_{12}** nanocluster. (a) Time-dependent UV-vis spectra of **Au_5Ag_{12}** in the CH_2Cl_2 solution; (b) Time-dependent UV-vis spectra of **Au_5Ag_{12}** in the solid state.

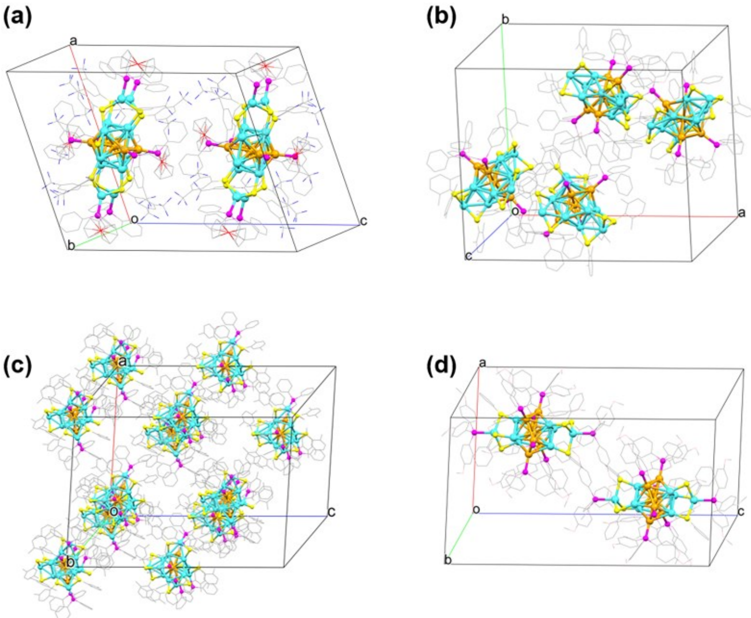

Figure S8. The unit cell the **Au_5Ag_{12}**, **Au_5Ag_{11}**, **Au_4Ag_{13}** and **Au_7Ag_8** nanoclusters. (a) **Au_5Ag_{12}**; (b) **Au_5Ag_{11}**; (b) **Au_4Ag_{13}**; (d) **Au_7Ag_8**. Color labels: orange = Au; light blue = Ag; red = Fe; yellow = S; magenta = P; pink = O; grey = C; white = H. All H atoms are omitted for clarity.

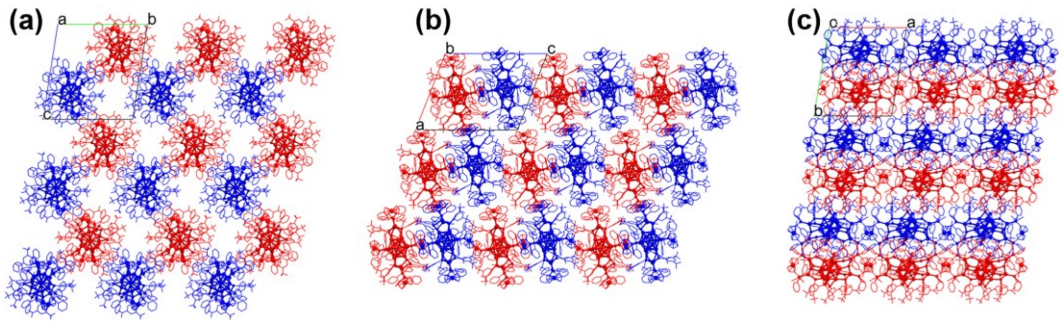

Figure S9. Packing mode of the **Au_5Ag_{12}** in the crystal shown. (a) Along the a axis; (b) Along the b axis; (c) Along the c axis. All H atoms are omitted for clarity. The cluster molecules arranged in different directions show in different colors.

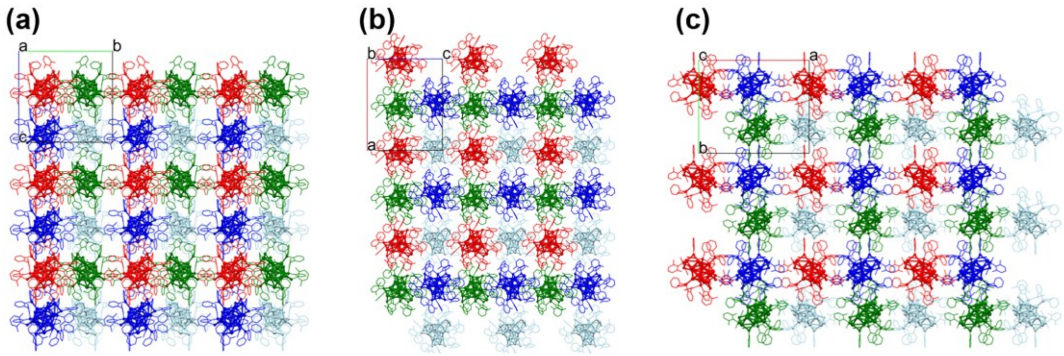

Figure S10. Packing mode of the **Au_5Ag_{11}** in the crystal shown. (a) Along the a axis; (b) Along the b axis; (c) Along the c axis. All H atoms are omitted for clarity. The cluster molecules arranged in different directions show in different colors.

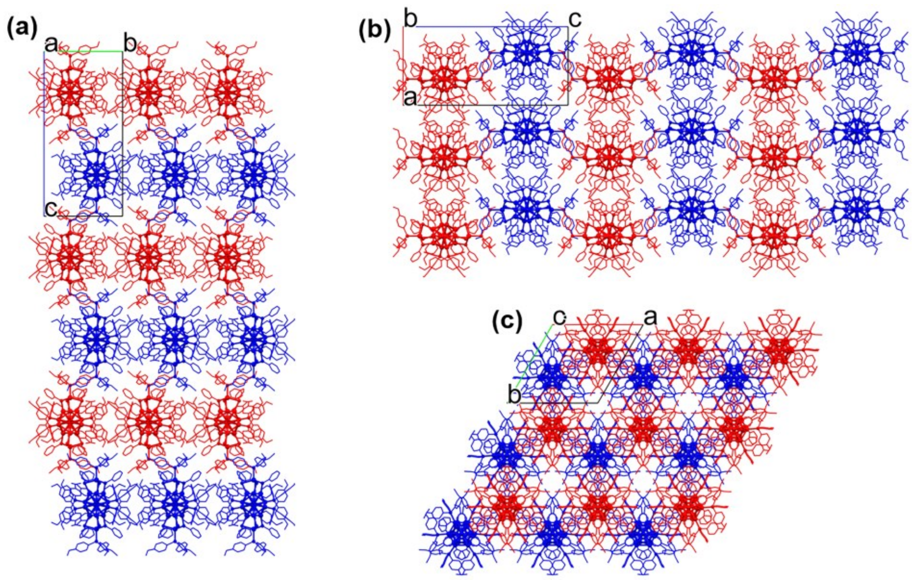

Figure S11. Packing mode of the **Au_7Ag_8** in the crystal shown. (a) Along the a axis; (b) Along the b axis; (c) Along the c axis. All H atoms are omitted for clarity. The cluster molecules arranged in different directions show in different colors.

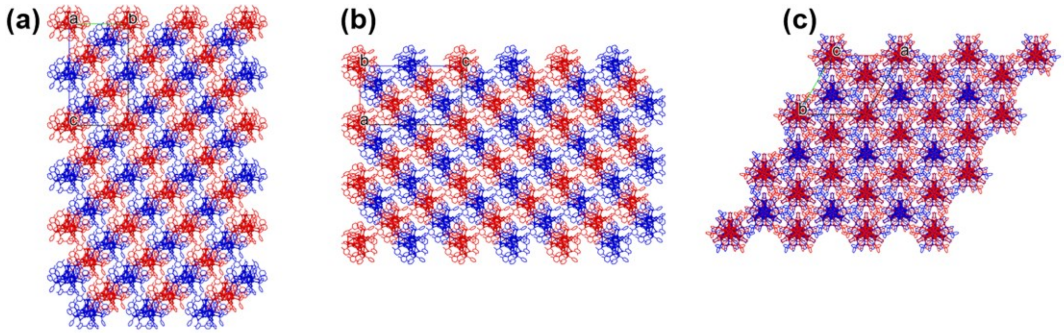

Figure S12. Packing mode of the **Au_4Ag_{13}** in the crystal shown. (a) Along the a axis; (b) Along the b axis; (c) Along the c axis. All H atoms are omitted for clarity. The cluster molecules arranged in different directions show in different colors.

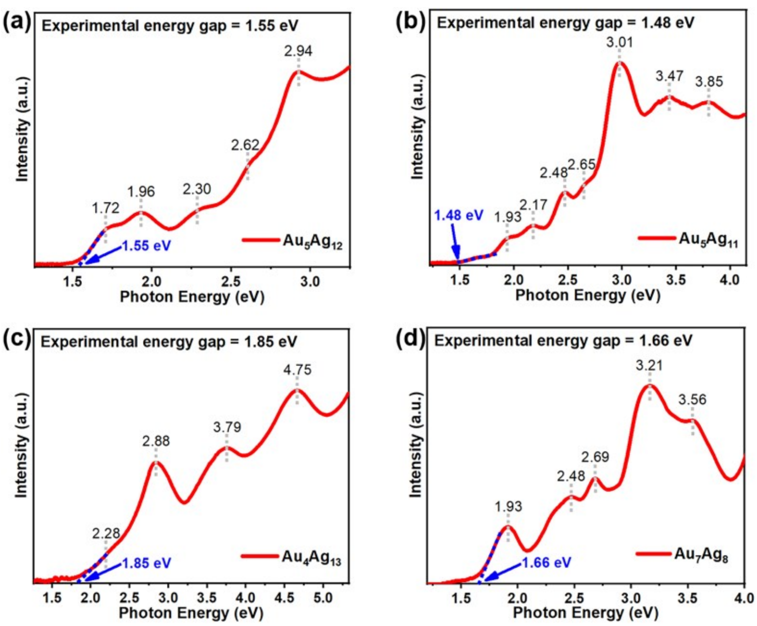

Figure S13. UV-vis absorption spectra (photon energy scale) of the **Au_5Ag_{12}**, **Au_5Ag_{11}**, **Au_4Ag_{13}** and **Au_7Ag_8** nanoclusters in CH_2Cl_2. (a) **Au_5Ag_{12}**; (b) **Au_5Ag_{11}**; (c) **Au_4Ag_{13}**; (d) **Au_7Ag_8**. The experimental energy gap of the **Au_5Ag_{12}**, **Au_5Ag_{11}**, **Au_4Ag_{13}** and **Au_7Ag_8** nanoclusters in CH_2Cl_2 was determined as ~1.55 eV, 1.48 eV, 1.85 eV, and 1.66 eV, respectively.

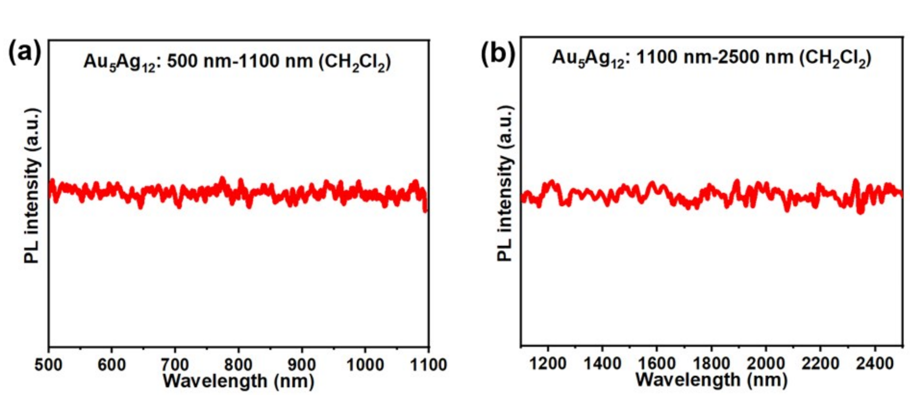

Figure S14. Photoluminescence spectra of **Au_5Ag_{12}** nanocluster in the CH_2Cl_2 solution at 300 K. (a) in 500-1100 nm range; (b) in 1100-2500 nm range.

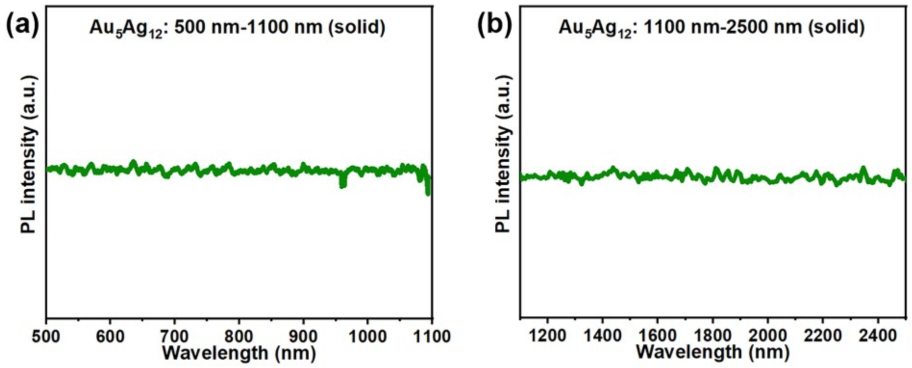

Figure S15. Photoluminescence spectra of $\mathbf{Au_5Ag_{12}}$ nanocluster in the solid state at 300 K. (a) in 500-1100 nm range; (b) in 1100-2500 nm range.

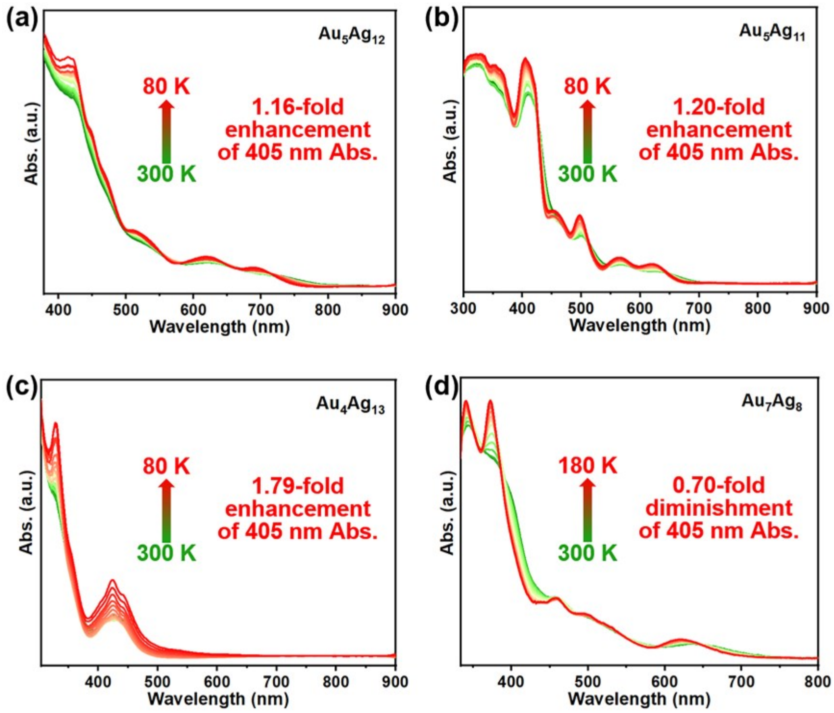

Figure S16. Temperature-dependent PL and UV-vis absorption spectra of $\mathbf{Au_5Ag_{12}}$, $\mathbf{Au_5Ag_{11}}$ and $\mathbf{Au_4Ag_{13}}$ nanoclusters in 2-MeTHF, and temperature-dependent PL and UV-vis absorption spectra of $\mathbf{Au_7Ag_8}$ nanocluster in acetone (from 300 K to 80 K, monitored per 10 K, λ_{ex} = 405 nm). (a) $\mathbf{Au_5Ag_{12}}$; (b) $\mathbf{Au_5Ag_{11}}$; (c) $\mathbf{Au_4Ag_{13}}$; (d) $\mathbf{Au_7Ag_8}$.

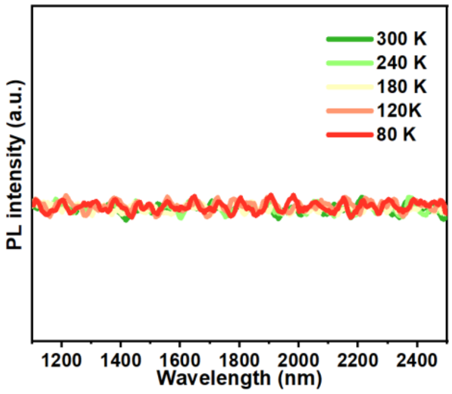

Figure S17. Temperature-dependent PL spectra of **Au_5Ag_{12}** nanocluster from 1100 nm to 2500 nm in 2-MeTHF from 300 K to 80 K (λ_{ex} = 405 nm).

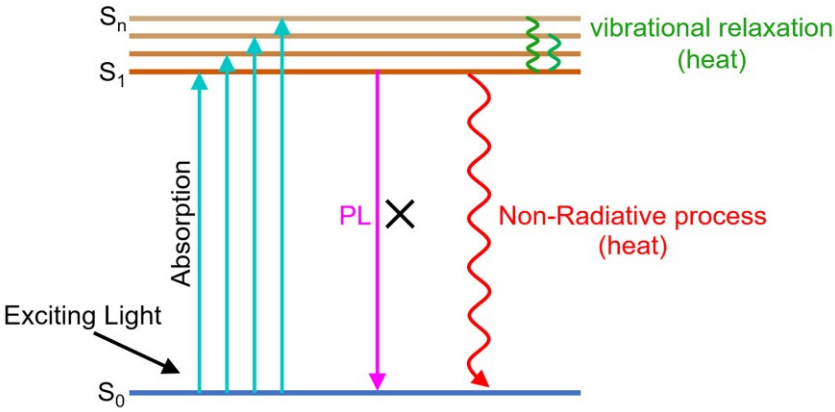

Figure S18. Simplified Jablonski diagram illustrating photophysical processes of **Au_5Ag_{12}** nanocluster. PL: photoluminescence.

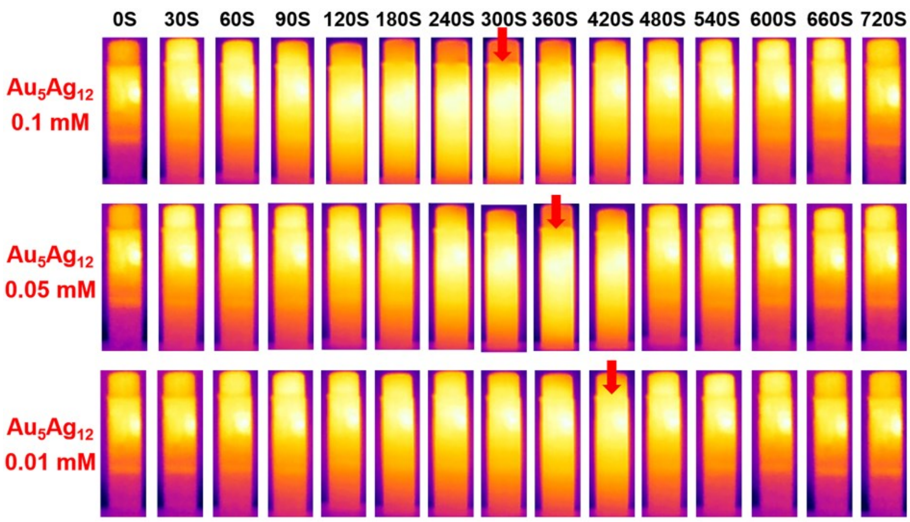

Figure S19. Time dependent images of **Au_5Ag_{12}** solutions of different concentrations (0.1 mM, 0.05 mM, and 0.01 mM) upon laser irradiation, followed by a cooling period (arrows indicate the time to stop irradiation).

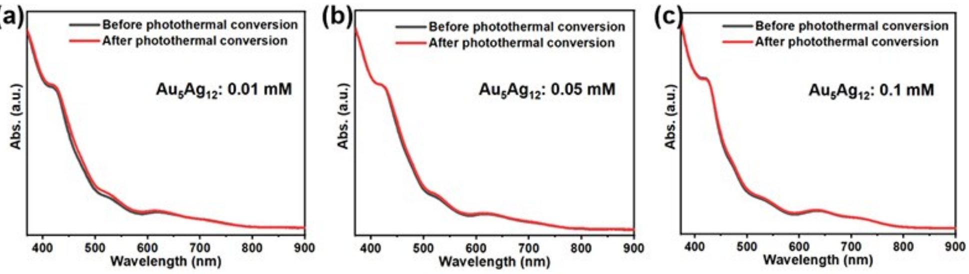

Figure S20. The photothermal stability of **Au_5Ag_{12}** nanoclusters at different concentrations was monitored by UV-vis spectroscopy. (a) 0.01 mM; (b) 0.05 mM; (c) 0.1 mM.

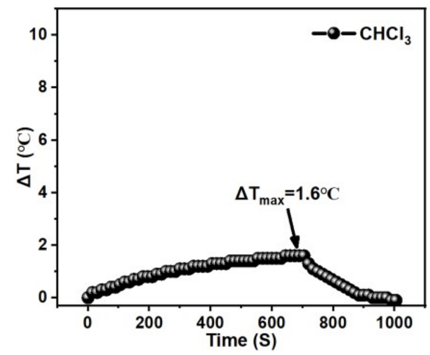

Figure S21. Temperature change of blank $CHCl_3$ solvent. Laser irradiation: 808 nm, 1.4 W cm^{-2}.

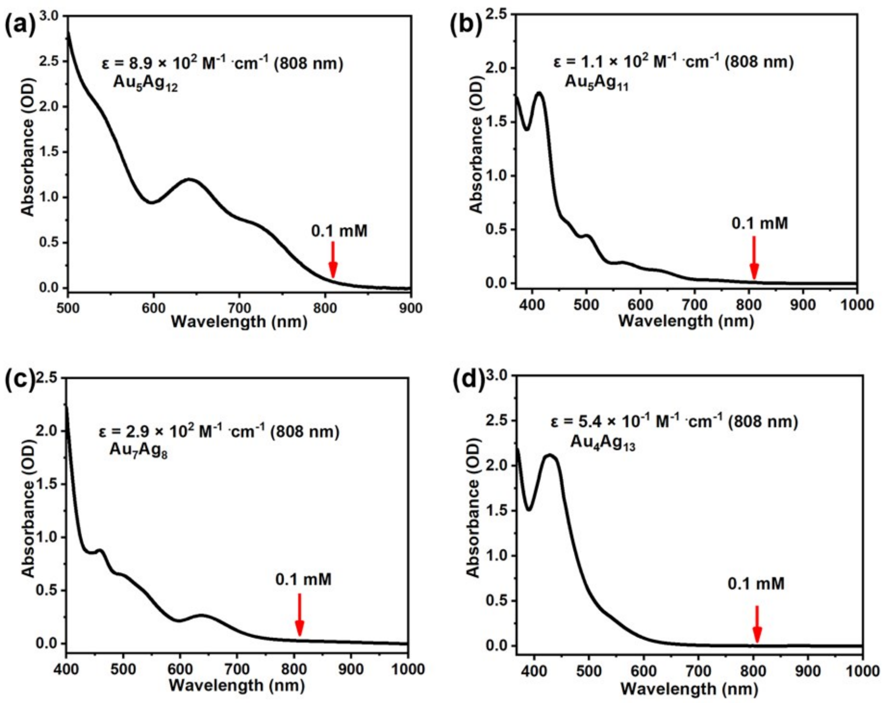

Figure S22. Absorption spectra of (a) **Au_5Ag_{12}**; (b) **Au_5Ag_{11}**; (c) **Au_7Ag_8** and (d) **Au_4Ag_{13}** dissolved in $CHCl_3$. Molar absorption coefficient ε is calculated by Beer's law: $A = \varepsilon \cdot c \cdot l$ (A is absorbance, c is the concentration of the solution (0.1 M), and l is the light length, i.e., 1 cm).

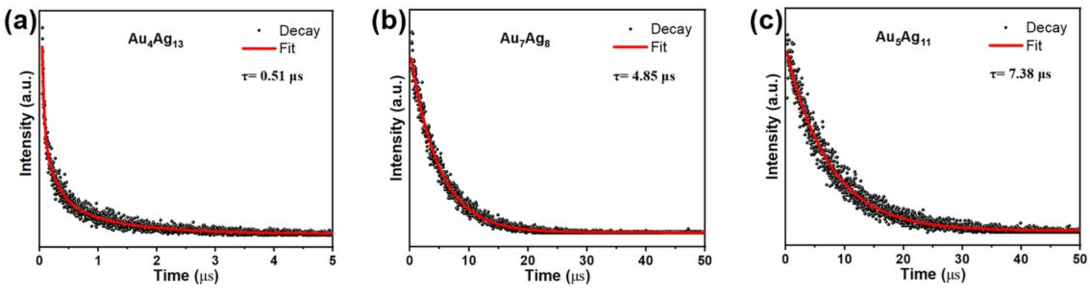

Figure S23. Fluorescence decay profile of $\mathbf{Au_4Ag_{13}}$, $\mathbf{Au_7Ag_8}$ and $\mathbf{Au_5Ag_{11}}$ nanoclusters. (a) $\mathbf{Au_4Ag_{13}}$; (b) $\mathbf{Au_7Ag_8}$; (c) $\mathbf{Au_5Ag_{11}}$.

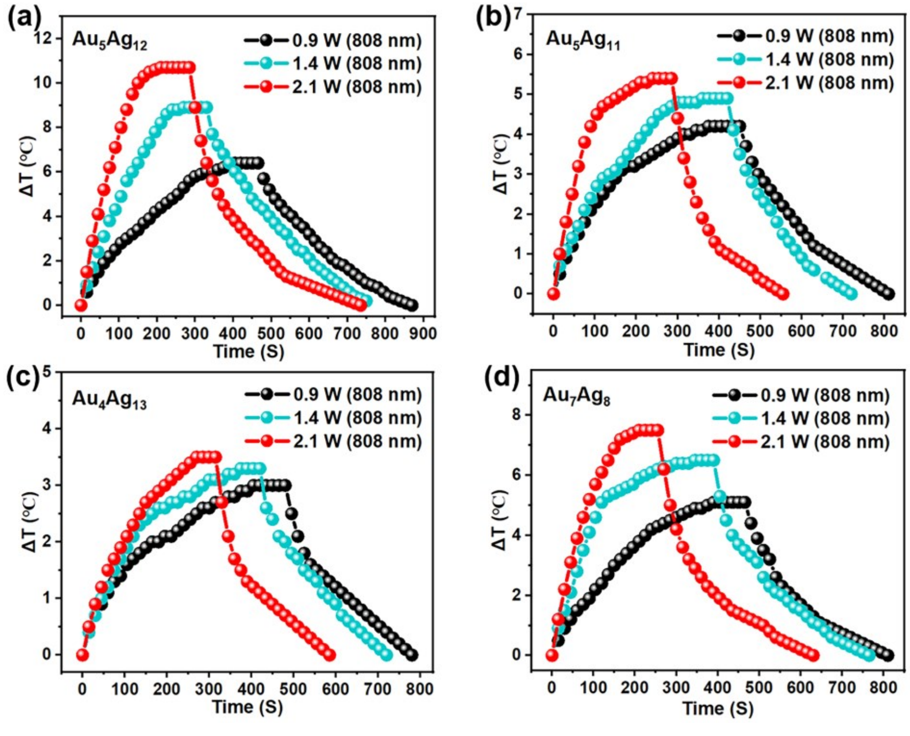

Figure S24. The time-dependent temperature of the four AuAg alloy nanoclusters solutions (0.1 mM) during laser irradiation at 808 nm with different power (0.9, 1.4, and 2.1 W cm^{-2}). (a) $\mathbf{Au_5Ag_{12}}$; (b) $\mathbf{Au_5Ag_{11}}$; (c) $\mathbf{Au_4Ag_{13}}$; (d) $\mathbf{Au_7Ag_8}$. Solvent: $CHCl_3$.

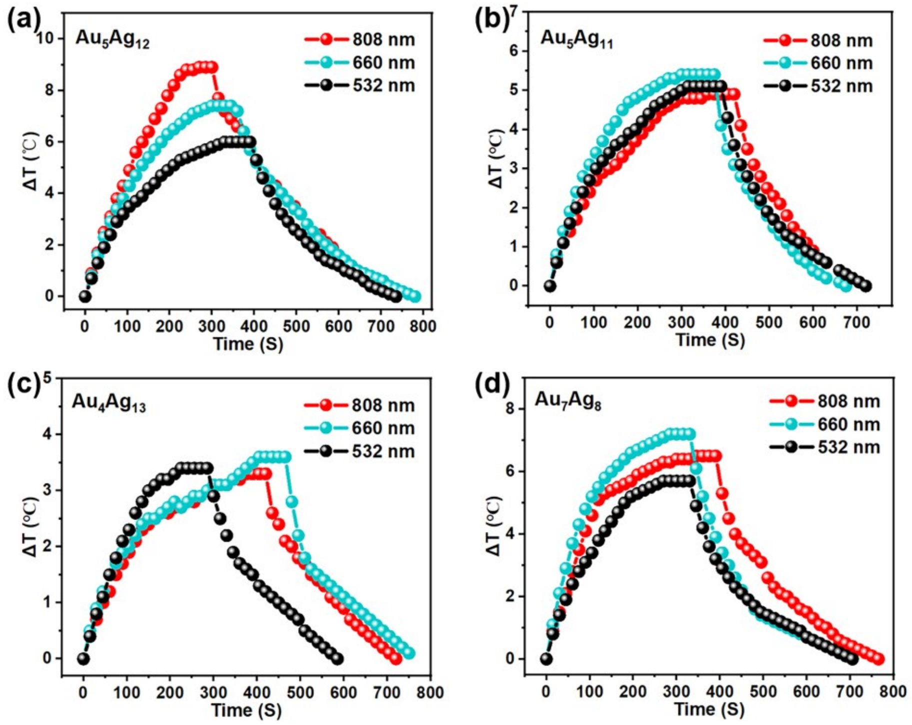

Figure S25. The time-dependent temperature of the four AuAg alloy nanoclusters solutions (0.1 mM) during laser irradiation at 1.4 W cm^{-2} with different wavelengths (808, 660, and 532 nm). (a) **Au_5Ag_{12}**; (b) **Au_5Ag_{11}**; (c) **Au_4Ag_{13}**; (d) **Au_7Ag_8**. Solvent: $CHCl_3$.

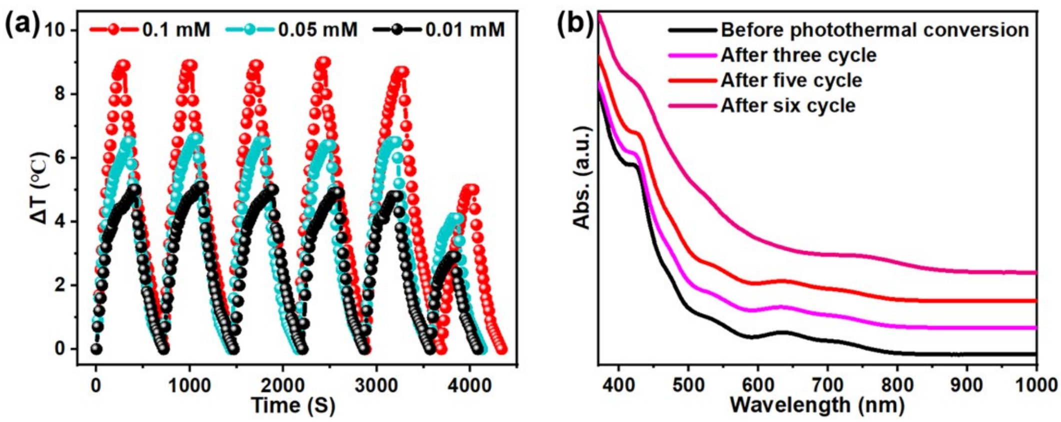

Figure S26. (a) Photothermal cycling measurement of **Au_5Ag_{12}** solutions (0.1 mM, red; 0.05 mM, cyan; 0.01 mM, black); (b) Corresponding UV-vis spectra of **Au_5Ag_{12}** (0.1 mM) after three cycles. Solvent: $CHCl_3$. Laser irradiation: 808 nm, 1.4 W cm^{-2}.

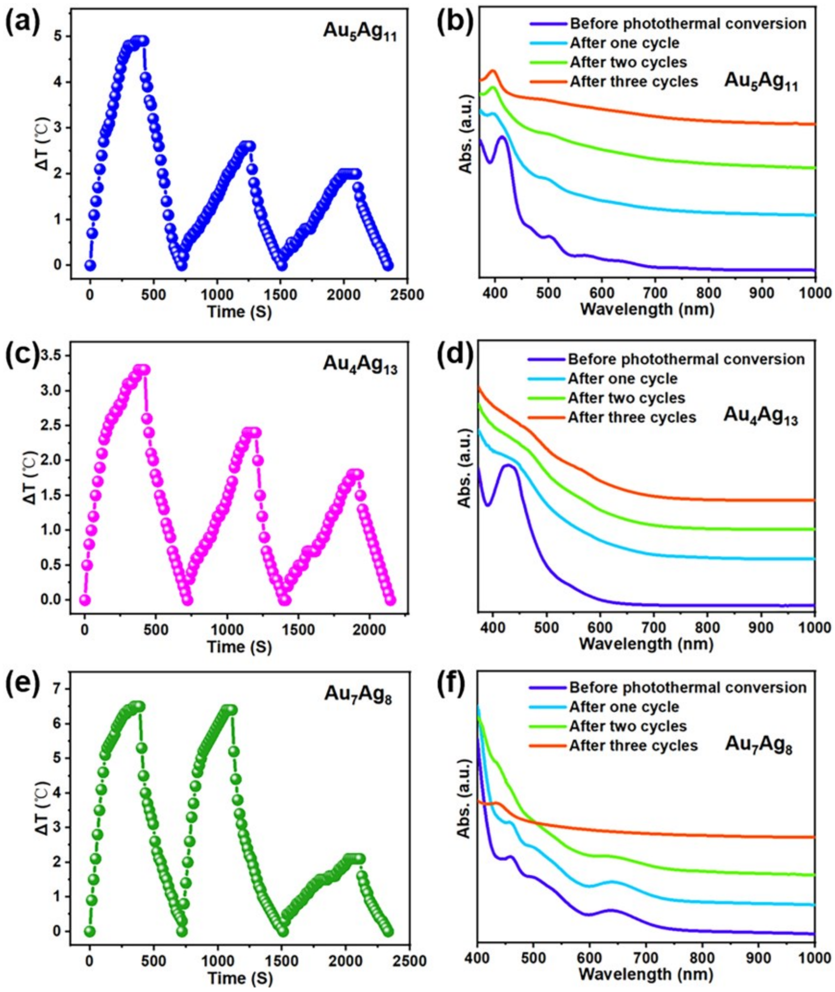

Figure S27. Photothermal cycling measurement and corresponding UV-vis spectra of $\mathbf{Au_5Ag_{11}}$, $\mathbf{Au_4Ag_{13}}$ and $\mathbf{Au_7Ag_8}$ nanoclusters in $CHCl_3$. (a) and (b) $\mathbf{Au_5Ag_{11}}$; (c) and (d) $\mathbf{Au_4Ag_{13}}$; (e) and (f) $\mathbf{Au_7Ag_8}$.

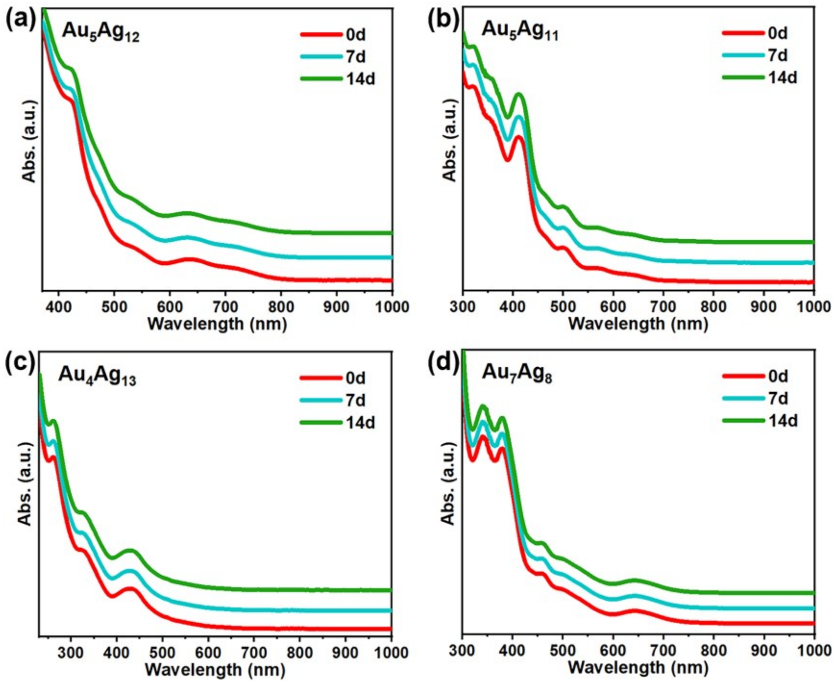

Figure S28. Monitoring the stability of $\mathbf{Au_5Ag_{12}}$, $\mathbf{Au_5Ag_{11}}$, $\mathbf{Au_4Ag_{13}}$ and $\mathbf{Au_7Ag_8}$ nanoclusters in $CHCl_3$ within 14 days. (a) $\mathbf{Au_5Ag_{12}}$; (b) $\mathbf{Au_5Ag_{11}}$; (c) $\mathbf{Au_4Ag_{13}}$; (d) $\mathbf{Au_7Ag_8}$.

Section 2. Supporting Table

Table S1. The crystal structure parameters for **$Au_5Ag_{12}(SR)_9(dppf)_4$**.

Empirical formula	$C_{208}H_{139}Ag_{12}Au_5F_{54}Fe_4P_8S_9$
Formula weight	6703.16
Temperature/K	150(2)
Crystal system	triclinic
Space group	$P\bar{1}$
a/Å	21.5917(4)
b/Å	23.5980(5)
c/Å	26.7319(5)
α/°	95.805(2)
β/°	110.205(2)
γ/°	97.054(2)
Volume/$Å^3$	12533.9(5)
Z	2
$\rho_{calc}g/cm^3$	1.776
μ/mm^{-1}	4.259
F(000)	6400.0
Radiation	Mo Kα (λ = 0.71073)
2Θ range for data collection/°	3.806 to 61.744
Index ranges	$-24 \leq h \leq 28$, $-29 \leq k \leq 33$, $-32 \leq l \leq 38$
Reflections collected	141631
Independent reflections	60287 [R_{int} = 0.0664, R_{sigma} = 0.0999]
Data/restraints/parameters	60287/3346/2701
Goodness-of-fit on F^2	1.093
Final R indexes [I>=2σ (I)]	R_1 = 0.0736, wR_2 = 0.1863
Final R indexes [all data]	R_1 = 0.1116, wR_2 = 0.2037
Largest diff. peak/hole / e $Å^{-3}$	5.64/-3.93

Table S2. The corresponding photoluminescence quantum yields (PLQY), fluorescence lifetimes (τ), radiative rate constants (k_R) and non-radiative rate constants (k_{NR}) of $\mathbf{Au_4Ag_{13}}$, $\mathbf{Au_7Ag_8}$, and $\mathbf{Au_5Ag_{11}}$ nanoclusters.

Nanocluster	**QY (%)**	**τ (μs)**	k_R **(s^{-1})**	k_{NR} **(s^{-1})**
$\mathbf{Au_4Ag_{13}}$	0.19	0.51	3.73×10^3	1.96×10^6
$\mathbf{Au_7Ag_8}$	1.62	4.85	3.34×10^3	2.02×10^5
$\mathbf{Au_5Ag_{11}}$	11.98	7.38	1.62×10^4	1.19×10^5